

# Design, Performance and Analysis of Thermal Lag of the UFS1 Twin-Calorimeter Chip for Fast Scanning Calorimetry using the Mettler-Toledo Flash DSC 1

Sander van Herwaarden<sup>1</sup>, Elina Iervolino<sup>1,4</sup>, Floor van Herwaarden<sup>1</sup>, Ties Wijffels<sup>2</sup>, Archi Leenaers<sup>2</sup>, Vincent Mathot<sup>3</sup>

<sup>1</sup> Xensor Integration, Delfgauw (The Netherlands); <sup>2</sup> Anatech, Sittard (The Netherlands);

<sup>3</sup> SciTe, Geleen (The Netherlands); <sup>4</sup> Delft University of Technology (The Netherlands).

## Abstract

This paper presents a new twin-membrane calorimeter chip for fast Differential Scanning Calorimetry (DSC) with the Flash DSC 1 of Mettler-Toledo. The thin silicon nitride membranes enable scan rates in excess of 10 kK/s in heating and up to 4 kK/s in cooling for sample masses between 100 ng and 10  $\mu\text{g}$  in the temperature range of -100  $^{\circ}\text{C}$  to 450  $^{\circ}\text{C}$ . The time constant for cooling is about 12 ms, the power resolution is typically 0.1- 0.5  $\mu\text{W}$ , the temperature accuracy of non-calibrated chips is typically better than  $\pm 5$  K. The paper also shows measurements for the scan-rate dependent thermal lag of the device, showing an empty sensor thermal lag of about 0.2 ms, and a mass dependent thermal lag of about 0.3 ms/ $\mu\text{g}$  for Indium for a good thermal contact between Indium and membrane.

**Key words:** Calorimeter Chip; Thermal Lag; Fast Scanning Calorimetry.

## Design

For the Flash DSC 1, an instrument recently (October 2010) introduced by Mettler-Toledo for Fast Scanning Calorimetry based on calorimeter chips [1], a new calorimeter chip has been developed. Where a lot of calorimeter chips sold so far are single cell types, for the Flash DSC a twin calorimeter chip was developed to enable differential measurements on the same chip. This has the advantage that sample and reference cell will be at the same temperature, and it also saves space. The development started with the following specifications in mind:

Scan Rate: 1-1000 K/s

Mass Range: 1-10  $\mu\text{g}$

Temperature Range: -100  $^{\circ}\text{C}$  to 400  $^{\circ}\text{C}$

Sample Pan: 1.8 mm  $\varnothing$

At first, a chip with a thick and robust silicon membrane was considered, conform the XEN-NCM-9924, see Fig.1 [2]. This chip will accept pans, and is robust enough to last the lifetime of the instrument.

However, the XEN-NCM9924 has a very limited accuracy of temperature measurement, since the thermal resistance of the membrane is not much larger than the thermal resistance from the chip's silicon frame to the ambient, both approximately 50 K/W. This makes that the cold junctions of the thermopile measuring the temperature increase of the sample area are not stable in temperature, and thus the measurement is complicated.

In total the thermal isolation is only 100 K/W, so that it would require 4 W to heat up the sensor to 400  $^{\circ}\text{C}$ . This is only the isothermal heat loss, for fast scanning additional power is required to heat up the membrane and sample. Besides, the integrated mono-silicon thermopile of this chip does not allow use up to 400  $^{\circ}\text{C}$  because the p-n junctions will start to leak above 180  $^{\circ}\text{C}$ .

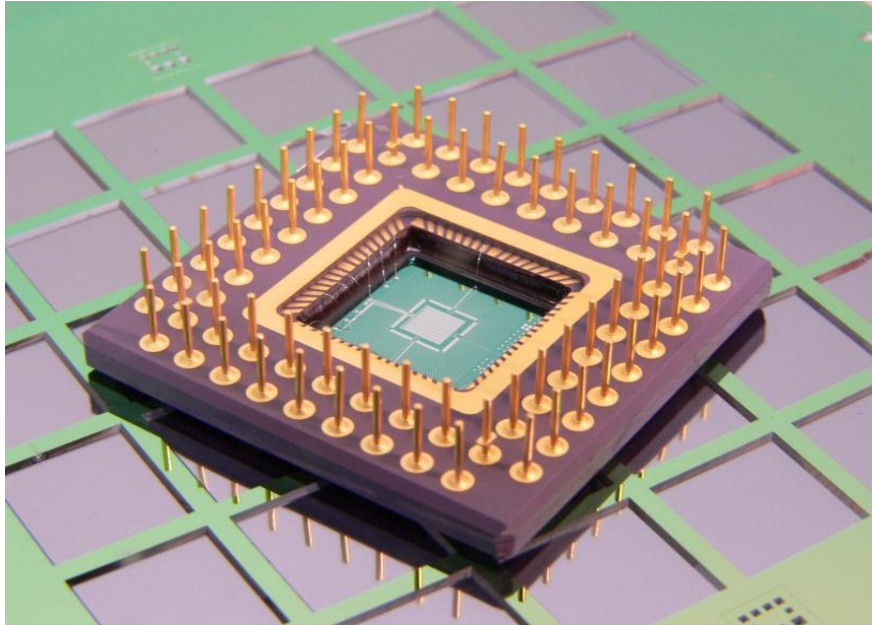


**Figure 1:** The XEN-NCM9924 with thick silicon membrane is robust, but not accurate and efficient for Fast Scanning Calorimetry (FSC) . Photograph courtesy [www.xensor.nl](http://www.xensor.nl).

Therefore the switch was made to another technology, based on low-stress silicon-nitride (SiN) thin membranes with poly-silicon thermopiles, that does not have these disadvantages [3], see Fig. 2.

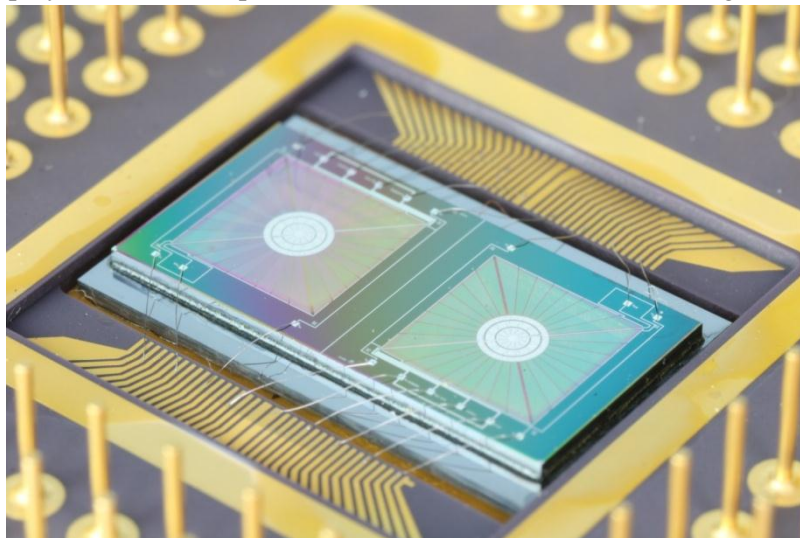


**Figure 2:** The chip XI-222, overall dimensions 15 mm × 7.5 mm, with twin silicon-nitride membranes 5×5 mm, aluminum-coated sample area 2 mm Ø, and poly-silicon thermopiles between the thick silicon frame and the sample area. Photograph courtesy [www.xensor.nl](http://www.xensor.nl).

The chip XI-222 is designed in this technology, with twin membranes of SiN and n-type/p-type poly-silicon thermopiles. This device has a thermal isolation to the ambient of the order of 2.5 kK/W, and the temperature increase of the cold junctions is now negligible. The sample area of this chip is 2 mm Ø, so that it will accept a sample pan of 1.8 mm Ø as was the initial specification.

However, experiments showed that using a pan for the sample leads to unpredictable behavior. The solution chosen to overcome this problem was to deposit the sample directly onto the membrane, just as what was already customary for other users of calorimeter chips.

Cleaning is usually not an option, because of the fragility of the sensor's thin membrane but, more strongly, because of the risk of cross-contamination with subsequent samples. This means that the calorimeter chip can only be used for one sample, which places strict limitations on the costs. So, the chip also has to be small, with an economic housing. This requirement is not met by the XI-222 chip, nor by the expensive 144-pins PGA housing.

This led to the design UFS1 (XI-400) ( $5.0\text{ mm} \times 3.3\text{ mm} \times 0.3\text{ mm}$ ) on the UFS1 ceramic base plate, see Fig. 3.

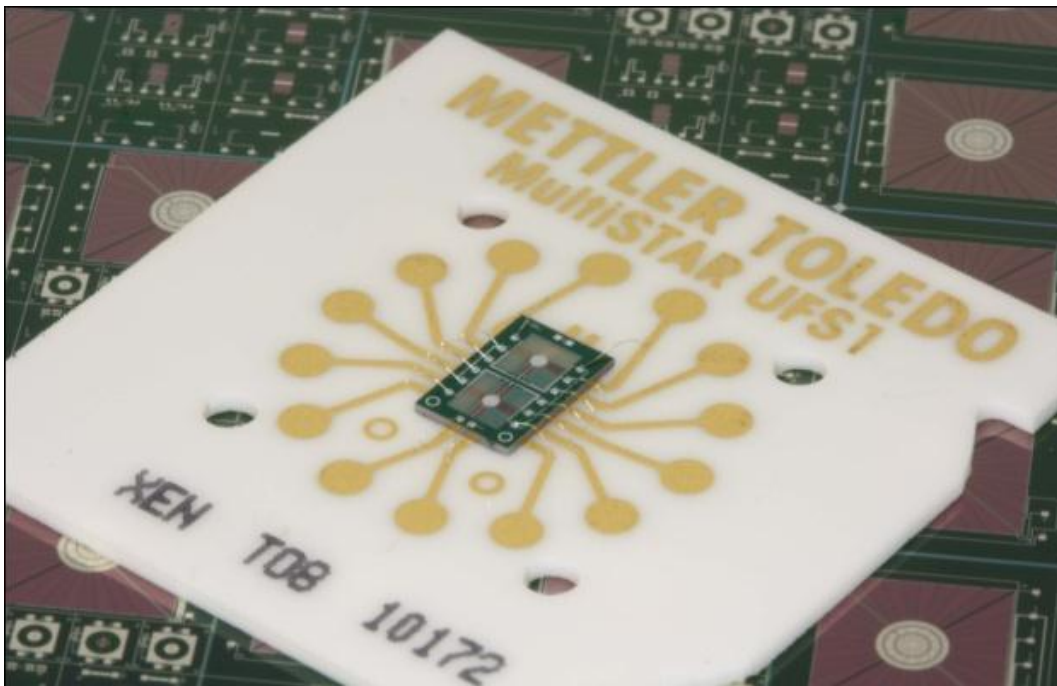


**Figure 3:** Photograph of the UFS1 calorimeter twin chip ( $5.0 \times 3.3 \times 0.3\text{ mm}^3$ ) and ceramic base plate ( $24 \times 24 \times 0.6\text{ mm}^3$ ). Photograph courtesy [www.xensor.nl](http://www.xensor.nl).

### Device description

The XI-400 chip ( $5.0\text{ mm} \times 3.3\text{ mm} \times 0.3\text{ mm}$ ) features two identical membranes of about  $1.6 \times 1.6\text{ mm}^2$  wide and about  $2\text{ }\mu\text{m}$  thick. It consists of silicon-nitride (SiN) and silicon oxide with in the middle a sample area of  $0.5\text{ mm}$  diameter, coated with aluminum (about  $0.5\text{ }\mu\text{m}$  thick) to attain a uniform sample-area temperature. There is a thermopile (with an internal resistance of about  $13\text{ k}\Omega$ ) to measure the sample area temperature, consisting of 8 p-type versus n-type poly-silicon thermocouples between the sample area and the  $300\text{ }\mu\text{m}$  thick silicon frame of the chip, that acts as heat sink, see Fig. 4.

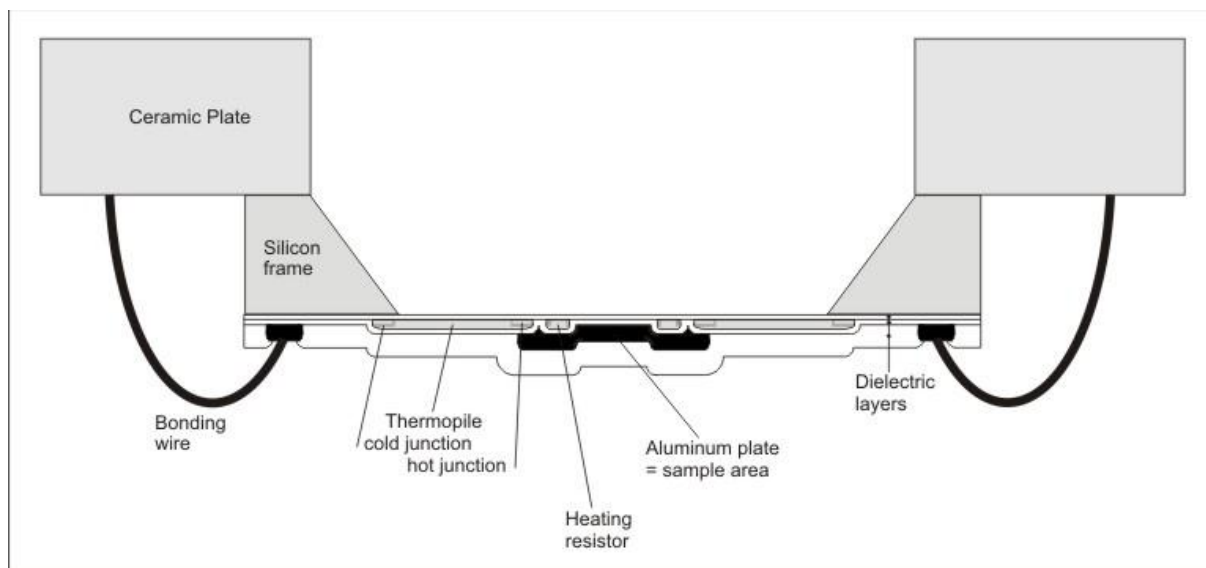


**Figure 4:** Schematic cross-section (not to scale) of the UFS1 ceramic+ chip (one membrane shown).

The sample area also has two heater resistances, a main heater (of about 5 kOhm) for realizing the general temperature scan program and a compensation heater (of about 4 kOhm) to compensate for temperature differences between the reference cell and the sample cell. Thus, the sensor is operated in a power compensation scheme.

The chip is mounted on a custom-designed ceramic base plate ( $24 \times 24 \times 0.6 \text{ mm}^3$ ) with 14 connection pads, using wire bonding.

## Performance

Below the performance of the device is presented. The batch of chips is factory pre-calibrated using an electrical method on a small number of randomly selected chips, which gives an indicative temperature calibration for all the chips of the batch [4]. This electrical pre-calibration is then checked by measuring the phase change temperature of Standard Reference Materials (SRM) such as a primary standard on another small number of chips [5], please consult [5] for an extensive description of the temperature calibration. Apart from this, users can apply an SRM on their own chips to further improve the accuracy of the temperature scale of the instrument, which is based on the electrical pre-calibration. This SRM can even be deposited on top of a sample such as a polymer, to check thermal lag within samples [6].

When carrying out an SRM-calibration, but also when simply working with the Flash DSC 1, the experimental settings, the sample, and the geometry and deposition details of the sample can have some influence on the temperature calibration. In this paper some measurements elucidating this for Indium are presented.

### Transfer and time constant

At room temperature the transfer of the device  $S$  in V/W (output voltage  $U_{tp}$  in V of the thermopile measuring the temperature difference between the sample area and the silicon frame of the device, see Fig. 4, divided by input power  $P$  in W, dissipated in the heating resistors in the sample area) is measured as about 24 V/W, and together with the thermopile sensitivity  $N\alpha_s$  of about 4 mV/K this means that the thermal isolation  $R_{th}$  between sample area and ambient, including thermal conduction by the surrounding air, is about  $24 \text{ V/W} / 4 \text{ mV/K} \approx 6 \text{ kK/W}$ , since:

$$S = U_{tp} / P = R_{th} \times N\alpha_s \quad (\text{V/W}) \quad (1)$$

These values are for room temperature, and dependent upon temperature.

Heating of the device by the instrument goes with a time constant of about 5 ms. The thermal RC time constant for cooling of the empty device  $\tau_c$  is of the order of 12 ms. With a value of  $R_{th} = 6 \text{ kK/W}$ , this means that the effective heat capacity of the sample area is about  $12 \text{ ms}/6 \text{ kK/W} = 2 \text{ } \mu\text{J/K}$ .

Considering that typically, the specific heat capacity of the materials making up the membrane (SiN, SiO<sub>2</sub>, poly-silicon and aluminum) is of the order of  $2 \text{ MJ/Km}^3$  [7], we can conclude that the volume which effectively participates in the heating and cooling of the device (for low frequencies, [8]) is equal to  $10^{-12} \text{ m}^3$  or a circle of 0.8 mm diameter at a membrane thickness of about  $2 \text{ } \mu\text{m}$ . So, beyond the actual sample area with a diameter of about 0.5 mm, only a small edge of about 0.15 mm beyond the sample area is effectively involved in the heating and cooling (under air atmosphere). Further away from the sample area, the temperature fluctuations are too small to be significant. This compares well with the values of 100-200  $\mu\text{m}$  that Minakov and Schick find for the effective enlargement of the sample area for calculating the sensor heat capacity (addenda) [8] in helium and nitrogen atmospheres. Such values can also be calculated doing numerical modeling with a simple EXCEL-sheet model. When working in a helium atmosphere, this edge will be smaller, effectively reducing the heat capacity of the device.

### Heating and Cooling rate

When the time constants are known the maximum heating and cooling rate can be estimated. For the heating, the maximum rate is limited only by the power that can be supplied by the electronics, and the maximum current that the heating resistor and its connecting tracks on the membrane can accommodate. For instance, if we assume that the instrument is capable of delivering just enough power to achieve a 450 K temperature increase, then the maximum heating rate would be around  $450 \text{ K} / 5 \text{ ms} = 90 \text{ kK/s}$ , which is reached almost immediately after initiating heating, and decreases linearly with temperature elevation to zero at 450 K temperature elevation.

For the cooling there is roughly a single-time-constant exponential behavior, and this  $\tau_c = R_{th} C_{mem}$  time constant limits the rate. At a given ambient temperature of the silicon frame  $T_{amb}$  the maximum cooling rate  $-dT/dt$  at any temperature  $T$  is given by:

$$-dT/dt = (T - T_{amb}) / \tau_c \quad (\text{K/s}) \quad (2)$$

With a typical time constant for cooling of 12 ms, and at a temperature elevation above  $T_{amb}$  of 240 K, the ballistic cooling rate will be about  $240 \text{ K} / 12 \text{ ms} = 20 \text{ kK/s}$ , decreasing linearly with the temperature elevation above  $T_{amb}$ .

So, the heating rate is maximum at zero temperature elevation, while the cooling rate is maximum at maximum temperature elevation.

### Power and Temperature resolution

The resolution of the device is limited by the Johnson noise of the thermopile internal resistance, which is about 13 kOhm. Then, the rms voltage noise  $u_n$  is given by:

$$u_n = \sqrt{4kTRB} \quad (\text{V}) \quad (3)$$

where  $k$  is Boltzmann's constant ( $1.38 \times 10^{-23} \text{ J/K}$ ),  $T$  is the absolute temperature in K,  $R$  is the thermopile electrical resistance, and  $B$  is the bandwidth, which is maximally 10 kHz, the sampling rate of the Flash DSC 1 instrument's ADC. In practice, the rms noise is often multiplied by a factor of 8 to

obtain the peak-to-peak noise  $u_{pp}$ . And if we take a more common sample rate of 400 Hz for a 100 K/s scan rate (in practice obtained by averaging 25 samples), we then arrive at a value at 300 K of:

$$u_{pp} \approx 8 \times \sqrt{(4kTRB)} = 8 \times \sqrt{(1200K \times 1.38 \times 10^{-23} J/K \times 13k\Omega \times 400Hz)} = 2.4 \mu V \quad (4)$$

Note that at a sample-area temperature of 450 °C, the noise is slightly higher because the average thermopile temperature  $T$  is higher. If we look at the peak-to-peak power noise  $p_{pp}$ , we need to divide the voltage noise by the transfer of the device:

$$p_{pp} \approx 2.4 \mu V / 24 V/W = 0.1 \mu W \quad (5)$$

These then are the numbers at room temperature for a sampling rate of 400 Hz. If the scan rate is very high, then no averaging is performed, and the noise level rises to its maximum at the maximum sample rate of 10 kHz:  $p_{pp} \approx 0.5 \mu W$ .

The noise voltage of 2.4  $\mu V$  is equivalent to a temperature noise of about  $2.4 \mu V / 4 mV/K = 0.6 mK$ .

Some main parameters of the calorimeter chip UFS1 (XI-400) are listed in Table 1, together with the initial target specifications.

**Table 1:** Main specifications of calorimeter chip UFS1 (XI-400) and initial target specifications.

Parameter	Value UFS1	Initial Specs
Membrane size [mm× mm]	1.6×1.6	
Sample Area [mm $\phi$ ]	0.5	1.8
Sample Pan	No	Yes (1.8 mm $\phi$ )
Mass range typically [ $\mu g$ ]	0.1 - 10	1-10
Thermal resistance [kK/W]	6	
Thermopile sensitivity [mV/K]	4	
Transfer [V/W]	24	
Time constant cooling [ms]	12	
Scan rate [K/s] heat typically	1 – 40 000	1 – 1000
Scan rate [K/s] cool typically	0.2 – 4000	1 – 1000
Temperature range [°C]	-100 to 450	-100 to 400

## Temperature Calibration by means of Electrical Pre-Calibration

Energy calibration of the XI-400 chip is in first order not required, since it is operated in power compensation. So, only temperature calibrations are given for the XI-400 chip. The temperature of the sample area could be determined using the heater elements directly, however, electronically it is easier to use the thermopile for the temperature measurement. This requires that the thermopile be calibrated, and this is done using the main heater elements [4, 5]. First, the resistance of the main heaters is calibrated versus temperature, and then, using the relationship between main heater resistance and temperature, a curve of  $U_{tp}$  versus  $T$  is made, which is valid for a specific ambient temperature  $T_{amb}$ . A typical  $U_{tp}$ -  $T$  curve of the thermopile, which shows a sensitivity of the order of 4 mV/K, is given in Fig. 5.

The accuracy of the resulting  $U_{\text{tp}}-T$  curve is checked using a number of test devices by determining the (extrapolated onset) phase change temperatures  $T_E$  of SRMs. The materials used for that include Adamantane, Indium, Tin and Zinc, with phase change temperatures of  $-64.5\text{ }^{\circ}\text{C}$ ,  $156.6\text{ }^{\circ}\text{C}$ ,  $231.9\text{ }^{\circ}\text{C}$  and  $419.5\text{ }^{\circ}\text{C}$ , respectively [5, 9].

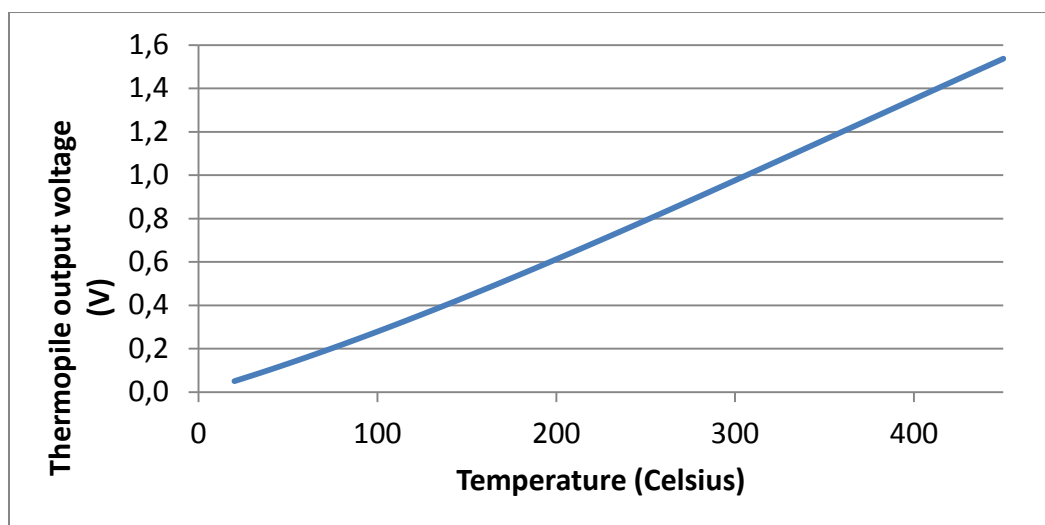


Figure 5: Thermopile output voltage versus sample-area temperature.

## Thermal Lag and other temperature deviations

Determining the  $T_E$  of a material is necessarily performed at a certain scan rate, in order to obtain a measurable power signal for the enthalpy change. It is generally found in DSC instruments that a thermal lag occurs, phenomena seem to occur at higher temperatures than they do at low heating rates [9]. In some materials such as polymers, phenomena can actually occur at a different temperature when using a different scan rate. In general the reason for the thermal lag is that the sample is at a lower temperature than the instrument's temperature sensor while heating (and at a higher temperature while cooling). This time lag (in s) multiplied by the heating rate (in K/s) gives a temperature lag (in K), and this is the reason for the apparent temperature increase.

Apart from the references [6], on the analysis of ultra-fast calorimeter chips and [9], on the analysis of thermal lag effects in fast traditional DSC instruments (Hyper DSC) some interesting literature on these phenomena can also be found in other papers. Very interesting in this respect is the new proposed DIN-specification on Temperature Calibration of Fast Scanning Calorimeters, [10], dealing exclusively with the task of calibration, and giving a lot of attention to the effects of thermal lag, since this effect makes a good temperature calibration more difficult. This specification also gives many interesting references. The paper by Winter and Hoehne describes a thermal-resistance/heat capacitance multi-element analysis of less well-isolated earlier-generation calorimeter chips [11]. The paper of Sarge et al [12] laid some of the foundations for the DIN-spec of [10] but then related to standard DSC. Finally, Alexander Minakov et al [13] give a rigorous mathematical description of their operation of one of the first well-isolated chip calorimeters.

In general we can distinguish several different contributions for the difference between the observed  $T_E$  and the value of the phase change as given in literature. Below we will deal with these contributions, treating them in a more approximative way than in Minakov's paper, but this will

suffice to get a first idea which phenomena play a role in causing the thermal lag, and what magnitude this effect is expected to be.

### **Systematic errors**

First of all, the combination of instrument and sensor chip may have systematic deviations, such as an error of the measurement of the silicon frame temperature  $T_{\text{amb}}$ , due to the inaccuracy of the Pt100 and the distance between the Pt100 and silicon frame. Furthermore, there can be systematic deviations in the sensor calibration curve.

### **Random errors**

Secondly, random errors in this measurement also occur. Apart from noise-like variations in voltage and (Pt100)-resistance measurements, which are usually small, an important cause of such errors is sensitivity differences between different sensor chips. The typical standard deviation in sensor transfer between the two membranes in a chip is found to be of the order of  $\pm 0.25\%$ , or  $\pm 1$  K in 400 K temperature increase.

### **Isothermal errors**

Thirdly, there are errors that we may call isothermal errors, errors that exist even at zero scan rate, and are not scan rate dependent. These errors are caused by the circumstance that the sample is at any time and scan rate at a different temperature than the thermopile hot junctions.

Such errors are caused by the heat flows in the sensor chip that occur when the chip is heated to an elevated temperature. All the conduction paths in and around the chip towards the ambient conduct heat when the temperature is elevated, creating the desired temperature increase. However, since the sample is usually not placed exactly on top of the hot junctions of the thermopile that measures the temperature increase of the sample area, heat flowing in the sample area can create temperature differences between the location of the sample and the location of the thermopile hot junctions. These are the isothermal errors, and they are created by thermal resistances within the membrane of the sample area, and also between the sensor's membrane and the sample (contact resistances). If the sample is at a reduced temperature because of this effect, the heat flow to the sample will be lower than expected (thus an apparent smaller specific heat capacity is measured), but the apparent  $T_E$  is higher, since the total energy required to heat the sample to the actual phase-change temperature is independent of the experimental set up.

Because these errors depend on a number of parameters, such as sample material, sample shape, sample position, thermal resistance of the sample area membrane, thermal contact resistance between sample and membrane, and also ambient gas conductivity and ambient temperature, it is very complex to model this. Figure 6 shows the melting point (extrapolated onset temperature of phase change during heating, here at 5 K/s) of various Indium samples of different mass, indicating a lot of scatter especially at low sample masses (below 10  $\mu\text{g}$ ). It appears that for heavier samples the apparent melting point is slightly higher, but also more stable. This would indicate that the isothermal errors are less predictable for the smaller samples.

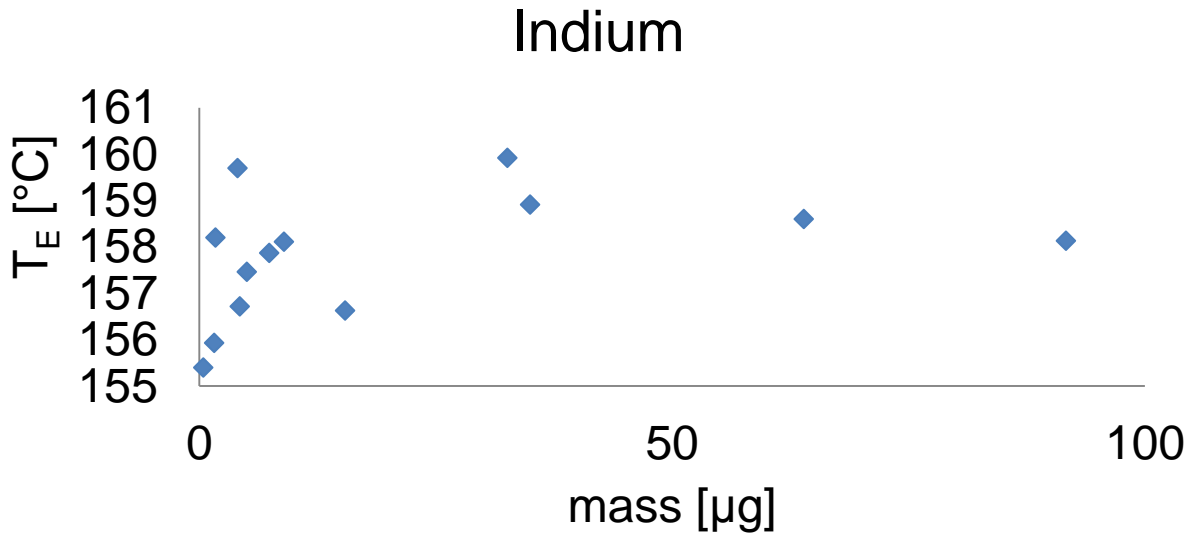


**Figure 6:** Extrapolated onset Temperature of melting of Indium for various samples of different mass.

#### Thermal Lag

Finally there is the thermal lag, which is scan-rate dependent and usually also, for a part, dependent upon the mass of the sample, because a larger sample has a larger thermal mass.

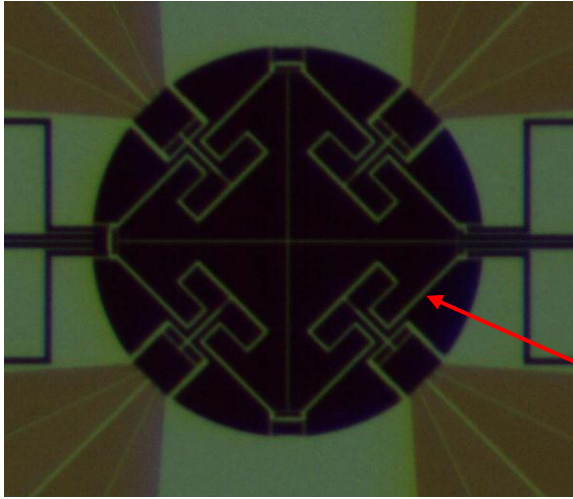
There are actually two effects in the sensor XI-400 leading to thermal lag, because of its extended size.

In general the thermal lag effects have been modeled by an international group defining a DIN-specification for the Temperature Calibration of Fast Scanning Calorimetry [10], and the DIN-specification gives the following general Equation to describe the thermal lag:

$$T_E(\beta, m) = a_0 + a_1 \beta^{a_2} + a_3 \beta m^{a_4} \quad (6)$$

In Eq. (6)  $\beta$  is the scan rate (in K/s),  $m$  denotes the mass of the sample (in kg), and the coefficients  $a_0$  to  $a_4$  are used for curve fitting to the experimental data. In general, the coefficient  $a_0$  can be equated to the literature value of the extrapolated onset of the phase change, that is to say, after eliminating the systematic and isothermal errors..

The second term of Eq.(6),  $a_1 \beta^{a_2}$ , describes the effect is that it takes some time to heat up the middle of the sample area via the main heater resistances located at the edge of the sample area. In particular, for lay-out reasons the aluminum plate covering the sample area (used to obtain a homogeneous temperature in the sample area) has a slit in it, to prevent short circuits between the various heaters, see Fig. 7. This slit is located between the main heaters and the middle of the sample area where the sample is usually deposited. And this slit has a relatively high thermal resistance of about 0.6 kK/W, since there in the absence of aluminum the conduction of heat is accomplished by the SiN dielectric layers only, and dominates the thermal resistance between main heaters and sample.



Slit in the aluminum plate on the sample area

**Figure 7:** Photograph of the sample area, with back-lighting, showing the slit in the aluminum plate (the bright line), which creates a significant thermal resistance between the main heater outside of the slit and the sample area center inside the slit. Photograph courtesy www.xensor.nl.

This thermal resistance, multiplied by the thermal mass of the center of the sample area, gives the time delay or thermal lag. If we estimate that the area within the slit occupies about  $1/6^{\text{th}}$  of the total sample area (which is including the edge of  $150\ \mu\text{m}$  beyond the aluminum circle of  $250\ \mu\text{m}$  radius), the thermal mass is also  $1/6^{\text{th}}$ , or  $2/6\ \mu\text{J/K}$ . So, this results in a time constant for this thermal lag effect of the order of  $0.6\ \text{kK/W} \times 0.33\ \mu\text{J/K} = 0.2\ \text{ms}$ . This  $0.2\ \text{ms}$  is described by the coefficient  $a_1$ . At this moment, we assume that the exponent  $a_2$  is unity, although further investigations might show that it should have a different value, especially for high scan rates ( $10\ \text{kK/s}$ ), because we see some non-linearity at high scan rates in Fig.9 even for the smallest samples (where the membrane heat capacity is the most important one).

This effect is present even if no sample is deposited onto the sample area, but a sample is needed to actually observe the effect. This is clearly shown in Figs. 8&9, where the thermal lag effects for the small samples all lie around the same lower limit.

The second thermal lag effect comes from the thermal resistance between compensation heater and sample  $R_{cs}$ , multiplied by the thermal mass of the sample, it is described by the last part of Eq.(6),  $a_3\beta m^{a_4}$ . The coefficient  $a_3$  is a time constant per mass, expressed in  $\text{ms}/\mu\text{g}$ . For exponent  $a_4$  we assume unity for now, although the experimental data at high scan rates ( $10\ \text{kK/s}$ ) show a sub-linear behavior of the thermal lag with scan rate.

This second effect is more difficult to model, since it depends not only on the sensor geometry, which is very well defined, but also on the sample mass, position, shape, characteristics, and thermal resistance between sample and sample area. Nonetheless we can endeavor to make an estimate of this effect. The thermal mass of the sample is simply its specific heat capacity  $c_p$  (in  $\text{J/kgK}$ ) multiplied by its mass  $m$  (in  $\text{kg}$ ). For Indium, which we use here as an example,  $c_p \approx 233\ \text{J/kgK}$  at room temperature. Then we need to make an estimate of the thermal resistance from compensation heater to sample. For this we will only observe the heat flow from compensation heater to sample, and assume that these are coupled (they indeed are by means of an electronic feedback system). We will treat the device as a linear system with two independent sources, the main heating program supplying the heat to set up the general temperature program of the device, and the compensation heating to supply or sink extra heat as needed by the sample. We analyze this system in two separate states, in which first the main heating is active and the compensation heating is zero, and then the other way around. According to the superposition theorem of network theory, we can then add these two states to get the whole picture.

In our case, the main heating program for the sample cell is prescribed by the main heating needed to keep the empty cell on the required temperature program. This then, with only a small inaccuracy induced by the presence of a sample slightly distorting the heat flow paths, sets up all the heat flows for the sample cell to follow the required temperature program.

As a consequence, the second state of the system, the compensation heating, only needs to supply power to the sample, and no heat flows to other parts of the system will occur. These have been taken care of by the first state. So, we can now proceed to calculate the thermal resistance between compensation heater and sample by evaluating the heat conduction paths between these two elements.

The compensation heater is located within the slit shown in Fig. 7, so the thermal resistance to the position where the sample is located is determined mainly by the aluminum plate between compensation heater and sample. This is in contrast to device designs where there is no aluminum on the sample area, and conduction through the gas cannot be neglected. Here, the presence of the aluminium plate on the sample area of device XI-400 makes the parallel heat conduction by air, helium or other gases around the sensor negligible for this heat conduction path. However conduction through the gas remains vital for the overall fast cooling of the sample area by transporting heat to the ambient. But here we have the luxury of a direct aluminum connection from heater to sample, and gas conduction in this second state of the system plays only a minor role. Eq. (7) gives a rough estimate of this thermal resistance of the aluminum between heaters and sample. For this we make the rough but easy approximations that the heaters are located on a circle with radius  $r_{\text{comp}}$  and the sample is in the center of the sample area with a sample radius of  $r_{\text{sam}}$ .

$$R_{\text{cs}} \approx R_{\text{sq}} \ln(r_{\text{comp}}/r_{\text{sam}})/2\pi \quad (\text{K/W}) \quad (7)$$

With a thermal sheet resistance of the aluminum layer of the order of 8 kK/W, and assuming a ratio of the radii of 2.7 (ca 150  $\mu\text{m}$  for the heater and 55  $\mu\text{m}$  for the sample), we arrive at the thermal resistance between compensation heater and sample of the order of 1.3 kK/W. If we use numerical modeling to obtain a precise value for this resistance, the value might be somewhat different, but since there are many badly known factors involved, this very simple model will serve to evaluate the size of this effect.

We can now determine the size of the coefficient  $a_3$ , which can be approximated by the product  $R_{\text{cs}} \times c_p \approx 233\text{J/kgK} \times 1.3 \text{ kK/W} = 300 \text{ ks/kg} = 0.3 \text{ ms}/\mu\text{g}$ .

In real life, however, the thermal contact between sample area membrane and sample is not ideal, and we need to add the thermal contact resistance  $R_{\text{cont}}$  that is present there to the thermal resistance of the aluminum. It is not very easy to model the contact resistance, so we can also turn things around, and look at the time constant that we actually obtain. This will allow us to estimate the size of the contact resistance, if we subtract the  $R_{\text{cs}}$  of about 1.3 kK/W.

We now arrive at the complete formula for the thermal lag for Indium:

$$T_E \approx T_{\text{lit}} + 0.2 \text{ ms} \times \beta + (R_{\text{mc}} + R_{\text{cont}}) \times c_{p \text{ sam}} \times \beta m \quad (8)$$

$$T_E \approx T_{\text{lit}} + \{0.2 \text{ ms} + m \tau_m\} \times \beta \quad (T_{\text{lit}} = 429.7485 \text{ K for Indium}) \quad (9)$$

Where  $\tau_m$  is the eventual mass dependent thermal lag time constant.

Fig. 8 shows the resulting thermal lag for four different samples of Indium, where the lines show the model, assuming a time lag of the membrane of 0.2 ms, for low scan rates up to 1000 K/s. The systematic, random and isothermal errors in  $T_E$  have been eliminated to end up with the 156.6 °C melting point for all curves at zero scan rate. Fig. 8 shows a fairly good linear behavior of the thermal lag with scan rate.

If we look at the actual thermal lag in K, and apply Eq. (9) to determine the value of  $\tau_m$  we get for the largest mass a value of about 9 K / 1000 K/s = 9 ms. By subtracting the 0.2 ms for the membrane we end up with 8.8 ms, or  $\tau_m \approx 8.8 \text{ ms} / 15 \mu\text{g} = 0.6 \text{ ms}/\mu\text{g}$ . Compared to the value of 0.3 ms in the absence of contact resistance, it seems that the contact resistance has an influence comparable to the aluminum resistance. For the mass of 9  $\mu\text{g}$ , the calculation gives a slightly smaller value of 0.5 ms/ $\mu\text{g}$ , and thus a slightly smaller contact resistance.

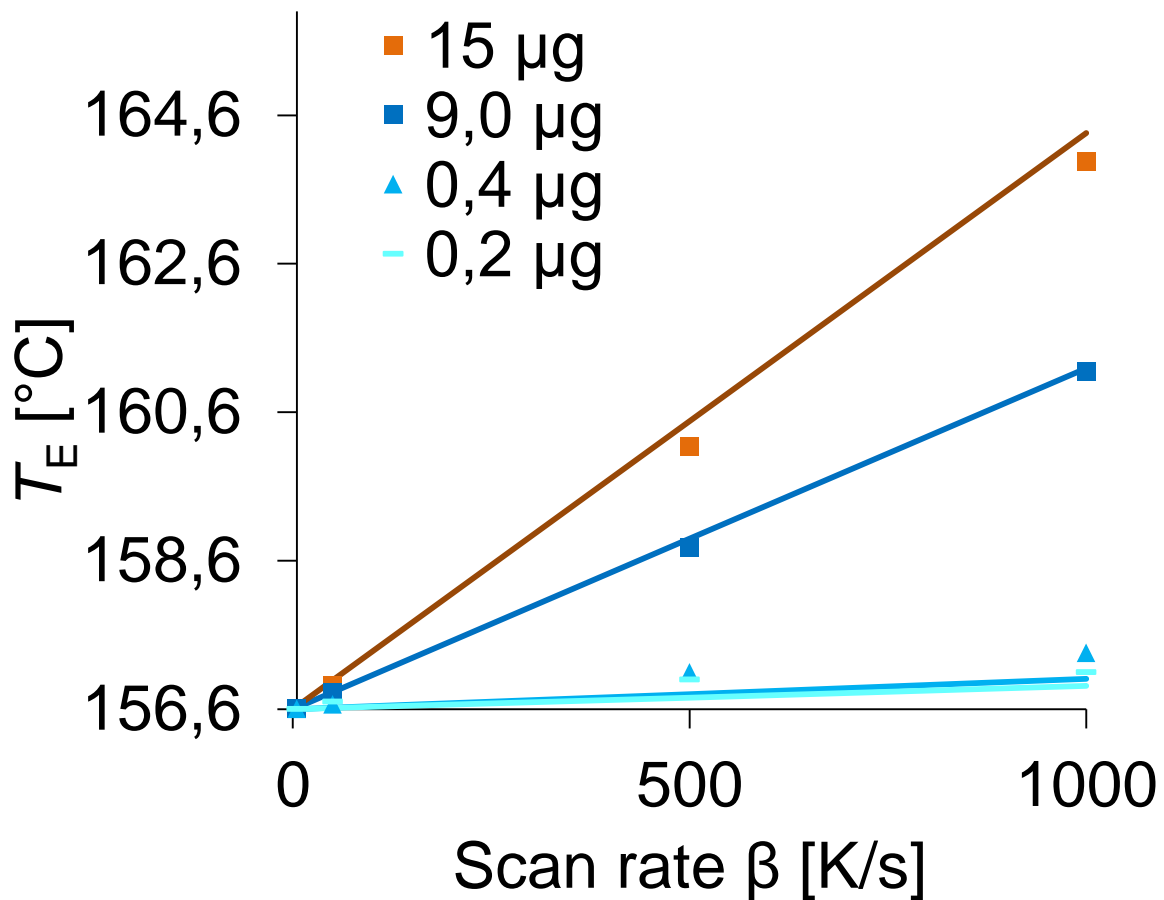


**Figure 8:** Thermal lag in the measurement of the melting of indium in air, for various sample sizes, points are measured values for various masses and scan rates, lines are the model including a thermal lag of 0.2 ms due to the heat capacity of the membrane.

In Fig. 9 values of  $\tau_m$  are given that have been calculated for the measurements shown there. The values indicate the presence of contact resistance, and the variations in these values show that these contact resistances are not very reproducible for metallic samples such as Indium. For polymers, the option exists for some materials to first melt the material to the membrane, this will give a much better thermal contact.

Fig. 9 also shows some sub-linear behavior of the thermal lag with scan rate for higher scan rates up to 10 000 K/s. A problem here is that in the formula for the DIN-spec 91127 there is the possibility to

describe non-linear behavior of the thermal lag with mass, but not with scan rate, while it appears that for this particular device we need to have this option. More measurements are required to arrive at the proper model, so that the DIN-spec formula may be improved to fit the behavior of this type of sensor.

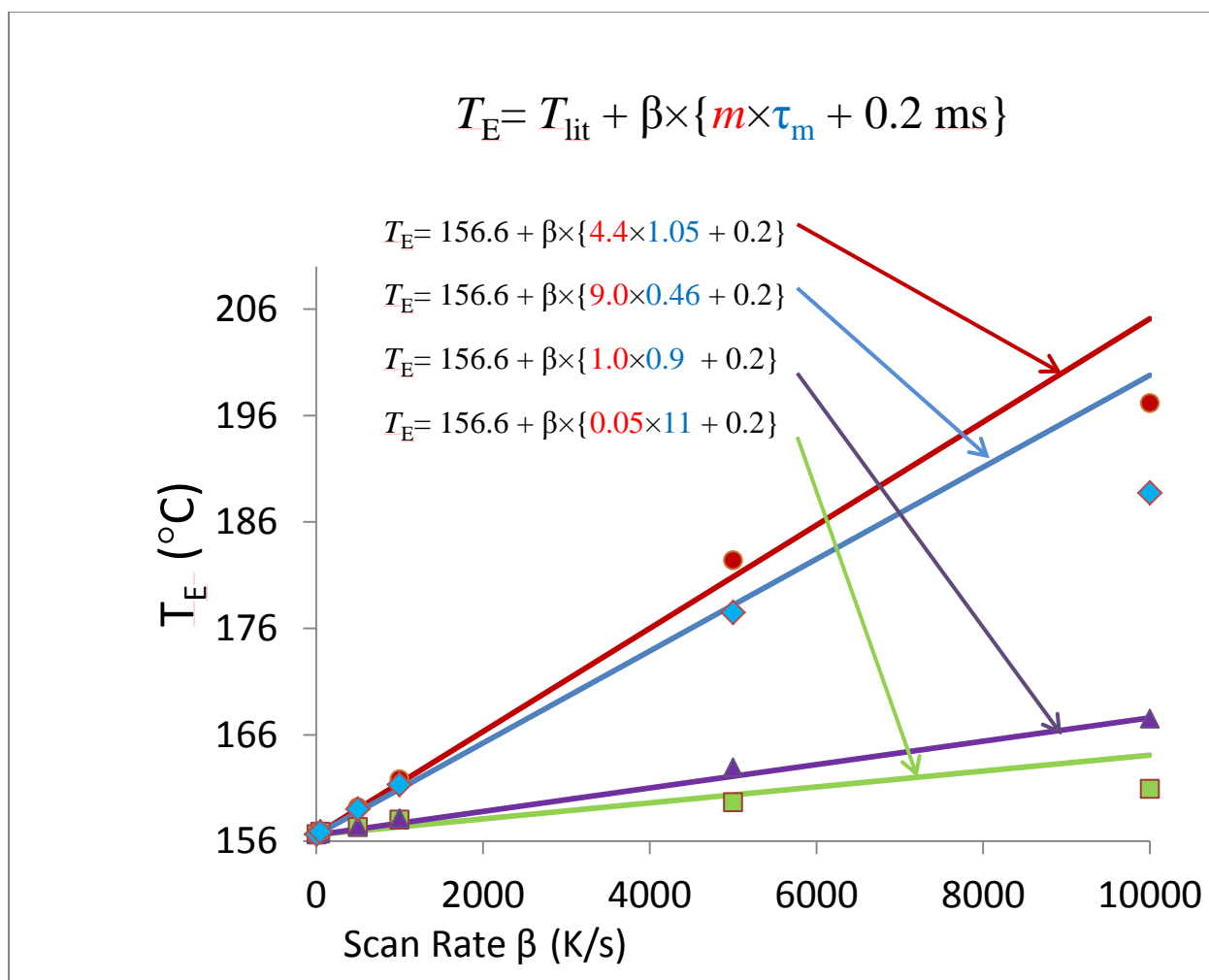


**Figure 9:** Thermal lag for Indium samples at higher scan rates, and noticeable thermal contact resistances, sample mass  $m$  indicated in red and thermal lag time constant  $\tau_m$  in blue (the expected value of  $\tau_m$  would be 0.3 ms/ $\mu$ g in case of a good thermal contact between sample and membrane). Also visible is a sub-linear dependence of thermal lag on scan rate at very high scan rates.

## Conclusions

We have presented a new calorimeter chip for fast scanning calorimetry, XI-400, to be used in a commercial instrument especially built around the chip (introduced in October 2010). The chip is intended for scanning calorimetric measurements at heating rates up to more than 10 kK/s, in a temperature range of -100 °C to 450 °C. Sample sizes are proportionally smaller than in standard DSC, down to 100 ng – 10  $\mu$ g. Because the sensor chip's own heat capacity is so much smaller than for DSC instruments, the so-called thermal lag is also comparable, only a few Kelvin at heating rates of the order of kK/s and  $\mu$ g samples.

## Acknowledgments

The authors want to thank SenterNovem (AgentschapNL) of the Dutch Ministry of Economic Affairs for their financial support under contract TSGE-3009. And they want to thank the staff of Xensor Integration and DIMES of Delft University of Technology for their technical support.

## References

- [1] Vincent Mathot, Marek Pyda, Thijs Pijpers, Geert Vanden Poel, Ernst van de Kerkhof, Sander van Herwaarden, Floor van Herwaarden, Archi Leenaers, The Flash DSC 1, a power compensation twin-type, chip-based Fast Scanning Calorimeter (FSC): first findings on polymers, *Thermochimica Acta*, this issue.
- [2] [www.xensor.nl](http://www.xensor.nl) Data sheet on XEN-NCM9924.
- [3] A.W. van Herwaarden, Overview of calorimeter chips for various applications, *Thermochimica Acta* 432 (2005) 192-201
- [4] E. Iervolino, A.W. van Herwaarden and P.M. Sarro, Temperature Calibration of Fast Scan Calorimeter Chips, *Proc. Euroensors XXII*, Dresden, Germany, (7-10 September 2008) 773-776
- [5] E. Iervolino, A.W. van Herwaarden, F.G. van Herwaarden, E. van de Kerkhof, P. van Grinsven, A. Leenaers, V.B.F. Mathot, P.M. Sarro, Temperature calibration and electrical characterization of the differential scanning calorimeter chip UFS1 for the Mettler-Toledo Flash DSC 1, *Thermochimica Acta*, This issue
- [6] E. Zhuravlev, C. Schick, Fast scanning power compensated differential scanning nanocalorimeter: 1. The device, *Thermochimica Acta* 505 (2010) 1-13
- [7] G.C.M. Meijer and A.W. van Herwaarden (editors), *Thermal Sensors*, Adam Hilger, Bristol (1994) ISBN 0-7503-0220-8, pp.287-288
- [8] Alexander A. Minakov and Christoph Schick, Ultrafast thermal processing and nanocalorimetry at heating and cooling rates up to 1 MK/s, *Rev. Sci. Instr.* 78 (2007) 073902 1-10
- [9] Geert Vanden Poel, Vincent B.F. Mathot, High-speed/high performance differential scanning Calorimetry (HPer DSC): Temperature calibration in the heating and cooling mode and minimization of thermal lag, *Thermochimica Acta* 446 (2006) 41-54
- [10] DIN Specification 91127 "Recommendation for Temperature Calibration of Fast Scanning Calorimeters" by the Research and Standardization Group of NaPolyNet, an FP7 program, see [www.napolynet.eu](http://www.napolynet.eu), to be published in 2011.
- [11] Werner Winter, Günther W.H. Höhne, Chip-calorimeter for small samples, *Thermochimica Acta* 403 (2003) 43-53
- [12] Stefan M. Sarge, Guenther W.H. Hoehne, Heiko K. Cammenga, Walter Eysel, Eberhard Gmelin, Temperature, heat and heat flow rate calibration of scanning calorimeters in the cooling mode, *Thermochimica Acta* 361 (2000) 1-20
- [13] A.A. Minakov, S.A. Adamovsky, C. Schick, Non-adiabatic thin-film (chip) nanocalorimetry, *Thermochimica Acta* 432 (2005) 177-185